Chemistry Simulation, and General Initial Value Problems, Computer Sciences and Systems Division, AERE Harwell, Oxfordshire.
Clore, G. M. (1983) in *Computing in Biological Science* (Geisow, M., & Barrett, A. N., Eds.) pp 314-348, Elsevier Biomedical Press, Amsterdam.
Dyson, H. J., Gippert, G. P., Case, D. A., Holmgren, A., & Wright, P. E. (1990) *Biochemistry 29*, 4129-4136.
Dyson, H. J., Tennant, L. L., & Holmgren, A. (1991) *Biochemistry 30*, 4262-4268.
Ebina, S., & Wüthrich, K. (1984) *J. Mol. Biol. 179*, 283-288.
Eklund, H., Gleason, F. L., & Holmgren, A. (1991) *Proteins 11*, 13-28.
Forman-Kay, J. D., Clore, G. M., Driscoll, P. C., Wingfield, P. T., Richards, F. M., & Gronenborn, A. M. (1989) *Biochemistry 28*, 7088-7097.
Forman-Kay, J. D., Gronenborn, A. M., Kay, L. E., Wingfield, P. T., & Clore, G. M. (1990) *Biochemistry 29*, 1566-1572.
Forman-Kay, J. D., Clore, G. M., Wingfield, P. T., & Gronenborn, A. M. (1991a) *Biochemistry 30*, 2685-2698.
Forman-Kay, J. D., Gronenborn, A. M., Wingfield, P. T., & Clore, G. M. (1991b) *J. Mol. Biol. 220*, 209-216.
Gleason, F. K., Lim, C.-J., Gerami-Nejad, M., & Fuchs, J. A. (1990) *Biochemistry 29*, 3701-3709.
Gregoret, L. M., Rader, S. D., Fletterick, R. J., & Cohen, F. E. (1991) *Proteins 9*, 99-107.
Holmgren, A. (1972) *J. Biol. Chem. 247*, 1992-1998.
Holmgren, A. (1989) *J. Biol. Chem. 264*, 13963-13966.
Holmgren, A. Söderberg, B.-O., Eklund, H., & Brändén, C.-I. (1975) *Proc. Natl. Acad. Sci. U.S.A. 72*, 2305-2309.
Honig, B., Sharp, K., Gilson, M., Fine, R., & Nicholls, A. (1988) *DelPhi—A Macromolecular Electrostatics Modelling Package*, Columbia University, New York.
Kallis, G. B., & Holmgren, A. (1980) *J. Biol. Chem. 255*, 10261-10265.
Katti, S. K., LeMaster, D. M., & Eklund, H. (1990) *J. Mol. Biol. 212*, 167-184.
Kohda, D., Sawada, T., & Inagaki, F. (1991) *Biochemistry 30*, 4896-4900.
Kraulis, P. J. (1991) *J. Appl. Crystallogr. 24*, 946-950.
Langsetmo, K., Sung, Y.-C., Fuchs, J., & Woodward, C. (1990) in *Current Research in Protein Chemistry: Techniques, Structure, and Function* (Villafranca, J., Ed.) pp 449-456, Academic Press, San Diego, CA.
Langsetmo, K., Fuchs, J. A., & Woodward, C. (1991a) *Biochemistry 30*, 7603-7609.
Langsetmo, K., Fuchs, J. A., Woodward, C., & Sharp, K. A. (1991b) *Biochemistry 30*, 7609-7614.
Marion, D., & Wüthrich, K. (1983) *Biochem. Biophys. Res. Commun. 113*, 967-974.
Nozaki, Y., & Tanford, C. (1967) *Methods Enzymol. 11*, 715-734.
Redfield, A. G., & Kuntz, S. D. (1975) *J. Magn. Reson. 19*, 250-254.
Reutimann, H., Straub, B., Luisi, P. L., & Holmgren, A. (1981) *J. Biol. Chem. 256*, 6796-6803.

Effects of Calcium Binding on the Internal Dynamic Properties of Bovine Brain Calmodulin, Studied by NMR and Optical Spectroscopy†

K. Török, A. N. Lane, S. R. Martin, J.-M. Janot,‡ and P. M. Bayley*
National Institute for Medical Research, Mill Hill, London NW7 1AA, U.K.
Received July 18, 1991; Revised Manuscript Received November 14, 1991

ABSTRACT: The dynamic properties of bovine brain calmodulin have been studied as a function of binding calcium ions, using a number of complementary spectroscopic methods. Rotational correlation times for proton–proton vectors within tyrosine and phenylalanine residues of calmodulin have been determined from time-dependent NOE measurements. In the presence of Ca^{2+}, a range of rotational correlation times is observed. The longest value is consistent with Ca_4–calmodulin having a markedly nonspherical shape in solution. In the absence of Ca^{2+}, the rotational correlation times of all vectors are significantly shorter, indicating that several phenylalanine side chains in apocalmodulin have increased internal dynamics. Time-resolved tyrosine fluorescence anisotropy shows global correlation times broadly in agreement with the NMR results, but with an additional faster correlation time [≈600 ps]. Tyrosine residues in apocalmodulin have substantial segmental motion, which becomes significantly reduced, but not eliminated, when Ca^{2+} is bound. The correlation time for global rotation of Ca_4–calmodulin increases from pH 7 to 4.5, indicating increased overall molecular asymmetry. This occurs without a significant change in total α-helix content as measured by circular dichroism. These results are consistent with the central region of Ca_4-calmodulin being relatively flexible in solution at pH 7, but with the molecule adopting a more extended shape under more acidic conditions. The Ca^{2+}-induced change in α-helix content can be mimicked by protonation. The α-helix content of Ca_4–calmodulin in solution appears less than in the crystal structure; additional α-helix is induced in partially nonaqueous solutions, particularly at acidic pH, as used in crystallization conditions.

Calmodulin is a ubiquitous intracellular Ca^{2+}-receptor protein which in the Ca^{2+}-loaded state can interact with and activate a number of protein kinases [see Klee (1988)]. The crystal structure of calmodulin (Babu et al., 1985, 1988; Kretsinger et al., 1986) shows that the protein consists of two Ca^{2+}-binding domains, each containing two E-F hand motifs, separated by an extended central α-helix to form a dumbbell-like shape. The mammalian protein contains two tyrosine residues but no tryptophan. Conformational changes involving

†The work was supported in part by EC Twinning Grant 852/00255/UK/05/PUJU1 (to P.M.B.) and the National Institutes of Health Grant 15835 to the Pennsylvania Muscle Institute.
*To whom correspondence should be addressed.
‡Present address: CNRS UA 330, 34033 Montpellier, France.

0006-2960/92/0431-3452$03.00/0

increased α-helical content, and changes in the environment of Tyr-99 (and particularly Tyr-138), occur when apo-CaM[1] binds Ca^{2+}, as shown by a number of spectroscopic techniques [reviewed in Klee (1980, 1988)]. Calmodulin can be cleaved by trypsin at Lys-78 to generate two domains (TR1C and TR2C) whose physical properties are very similar to those of the intact protein, suggesting that the two halves of the molecule are effectively independent structures (Aulabaugh et al., 1984; Dalgarno et al., 1984; Ikura et al., 1987; Thulin et al., 1984; Martin et al., 1985, 1986). The fragments generally have weaker activating effects on target proteins; thus the whole calmodulin molecule is generally necessary for full biological function (Newton et al., 1984).

The persistence of a long central α-helix in Ca_4–CaM in solution has been questioned recently. The α-helical content of Ca_4–CaM, as estimated by CD, appears in many studies to be significantly less than the value of 67% inferred from the crystal structure [see Martin and Bayley (1986), but cf. Hennessey et al. (1987)]. Further, small-angle X-ray scattering studies (Heidorn & Trewhella, 1988) gave a distance-distribution function for Ca_4–CaM which was better modeled with the central α-helix being bent. An explicit model with bending at residue 81 was proposed by Persechini and Kretsinger (1988a,b) from chemical cross-linking of an engineered calmodulin mutant, and results consistent with this were obtained from photo-cross-linking calmodulin with model peptides (O'Neil et al., 1989; O'Neil & Degrado, 1990). SAXS and SANS results on Ca_4–CaM in the presence of different peptides show that the calmodulin–peptide complexes can adopt either collapsed or extended shape, consistent with a hinged or flexible structure for calmodulin in the complex (Heidorn et al., 1989; Kataoka et al., 1989; Matsushima et al., 1989; Trewhella et al., 1990). Further, recent NMR results indicate a discontinuity in the central α-helix following residues 78–81 (Ikura et al., 1991a,b).

By contrast, time-resolved fluorescence studies using intrinsic chromophores, such as the photo-cross-linked tyrosine dimer (Small & Anderson, 1988) or tyrosine itself (Gryczynski et al., 1988, 1991), have been interpreted in terms of the dumbbell model, mainly on account of the global rotational correlation time being significantly longer than the 6–7 ns calculated for a hydrated sphere of M_r 16000 (Cantor & Schimmel, 1980). Previous studies using tyrosine fluorescence (Bayley et al., 1988) indicated that apocalmodulin appears to have a compact structure, with more pronounced internal dynamics compared with Ca_4–CaM.

In the present work, we have used ^{1}H NMR, fluorescence, and CD methods to investigate the dynamic and conformational changes in mammalian calmodulin induced by binding Ca^{2+}. There are several well-resolved resonances in the aromatic region of the NMR spectrum (Seamon, 1980; Ikura et al., 1983a,b, 1984; Klevit et al., 1984; Dalgarno et al., 1984; Thulin et al., 1984) that are ideal for measuring effective rotational correlation times (Dobson et al., 1982; Lane et al., 1986; Lane, 1989) independent of internal rotations about the $C_\beta C_\gamma$ bond. These residues include Tyr-99 and Tyr-138, whose dynamics can be monitored independently by time-resolved fluorescence.

Combining the results from these complementary spectroscopic techniques indicates that, at neutral pH, the tyrosine residues in apocalmodulin show a relatively mobile structure; on binding Ca^{2+}, motion of tyrosine side chains is significantly restricted, and there is a pronounced increase in the apparent hydrodynamic volume. Ca_4–CaM adopts a more extended structure as the pH is lowered. These results support the view that Ca_4–CaM itself shows substantial flexibility in the central region of the molecule, and this is dependent upon local environmental conditions. This property may be of significance in the ability of calmodulin to interact specifically and with high affinity with a range of different target sequences.

Materials and Methods

Protein Purification. Calmodulin was purified from bovine brain by chromatography on DEAE-cellulose and phenyl-Sepharose (Gopalakrishna & Anderson, 1982). After removal of the outer membranes, the brains were homogenized in a Waring blender with 4 volumes of buffer A (20 mM Tris·HCl, pH 7.5), containing 1 mM EGTA and 1 mM EDTA. The homogenate was centrifuged at 20000*g* for 20 min at 4 °C. The pellets were homogenized and centrifuged in the same way. The supernatants were combined, filtered through two layers of cheesecloth, and then mixed with 400 mL of a slurry of DEAE-cellulose (DE-52, Whatman) equilibrated in the same buffer and stirred for 10 min at 4 °C. After being washed on a sintered glass filter, the DEAE-cellulose was poured into a column (3.5 × 40 cm). Protein was eluted using a gradient from 0 to 1 M NaCl (2 L). Fractions were assayed for calmodulin activity by phosphodiesterase activation (Schiefer, 1985). Calmodulin elutes typically at 0.3–0.5 M NaCl. Active fractions were pooled and made 5 mM in $CaCl_2$. The solution was warmed to 30 °C and stirred for 15 min with 200 mL of phenyl-Sepharose (equilibrated with buffer A, containing 1 mM $CaCl_2$). After being washed with 2 L of the same buffer, the phenyl-Sepharose was poured into a column (3.5 × 20 cm) and cooled to 4 °C. Calmodulin was eluted with a buffer containing 2 mM EGTA and 2 mM EDTA. The protein was purified to homogeneity by FPLC on a Mono-Q column in the buffer system used for DEAE-cellulose chromatography. This step is used to resolve calmodulin from the closely related S-100 proteins (Yazawa et al., 1980). The purified calmodulin was desalted by gel filtration and lyophilized.

Ca_4–CaM (2.5 mL; 10 mg/mL) was prepared for NMR spectroscopy by adding $CaCl_2$ to 2.5 mM. The sample was passed down a PD-10 column equilibrated with 14.3 mM KCl, at pH 7.0, and lyophilized. The protein was then dissolved in 0.5 mL of D_2O or H_2O, to a concentration of 3 mM in 100 mM KCl, pH 7.0. The pH was changed by addition of DCl to the sample in the NMR tube. Atomic absorption spectroscopy showed that the sample contained 4.4 mol of Ca^{2+} per mol of calmodulin.

Apo-CaM was prepared for NMR as follows: a stock solution of Ca_4–CaM was desalted on a PD-10 gel filtration column equilibrated in water. The pH of this solution was adjusted to 2 (with 1 M HCl), where the affinity for Ca^{2+} is low and the protein remains soluble at low ionic strength (Haiech et al., 1981). The solution was passed through a PD-10 column in 10 mM HCl, the pH was adjusted to 7.0 with KOH, KCl was added to 4.3 mM, and the sample was then lyophilized. The powder was then prepared for NMR analysis

[1] Abbreviations: NOESY, nuclear Overhauser enhancement spectroscopy; DQF-COSY, double-quantum filtered correlated spectroscopy; TPPI, time-proportional phase incrementation; HOHAHA, homonuclear Hartmann–Hahn; SCUBA, stimulated cross-peaks under bleached alphas; SAXS, small-angle X-ray scattering; SANS, small-angle neutron scattering; CD, circular dichroism; Mes, 2-(*N*-morpholino)ethanesulfonic acid; EGTA, [ethylenebis(oxyethylenenitrilo)]tetraacetic acid; TFE, 2,2,2-trifluoroethanol; CaM, calmodulin; Ca_4–CaM, calmodulin in the presence of excess Ca^{2+} when all four calcium-binding sites are occupied; apo-CaM, calmodulin, in which the removal of Ca^{2+} by pH 2 treatment has been demonstrated by atomic absorption spectroscopy; EGTA–CaM, calmodulin in the presence of excess EGTA, when, as shown in the text, other cations may be bound; MLCK, myosin light-chain kinase.

in the same way as for Ca_4–CaM. The Ca^{2+} content (measured by atomic absorption spectroscopy) was <0.03 mol/mol calmodulin i.e., <1% of the calcium-binding site concentration. Protein concentration was estimated for apo-CaM using an absorbance at 277 nm of 3300 M^{-1} cm^{-1} (Klee, 1977).

NMR Spectroscopy. Calmodulin solutions were 3 mM in 100 mM KCl. Solutions in D_2O were at pD* 7.0 (equivalent to pH 6.6), and in H_2O the pH was 5.9. One-dimensional spectra were recorded at 15, 25, and 40 °C using a spectral width of 5000 Hz and 16 384 data points. Truncated one-dimensional NOE experiments were performed with 16 acquisitions on and off resonance, as described by Wagner and Wüthrich (1979). NOESY, DQF-COSY, and HOHAHA spectra were recorded in the phase-sensitive mode using TPPI (Marion & Wüthrich, 1983), in which sine-modulated data were collected (Frenkiel et al., 1990). Spectra in D_2O at 400 MHz were recorded with a 4-kHz spectral width using 2048 points in F_2 and 512 in F_1. The data matrices were zero-filled to 4096 by 2048 points prior to Fourier transformation. Spectra in H_2O were recorded at 500 MHz with a spectral width of 6.5 kHz, with 4096 points in F_2 and 512 points in F_1. The intense H_2O signal was suppressed by presaturation with the decoupler phase coherent with the receiver and using SCUBA to recover bleached α-carbon resonances. HOHAHA spectra were recorded with a spin-lock field of 7.9 kHz generated with an MLEV-17 sequence (Bax & Davis, 1985).

One-dimensional NOE time courses were analyzed by nonlinear regression as previously described (Lane et al., 1986). The apparent correlation times τ were derived from the cross-relaxation rate constants according to

$$\sigma = 56.92\tau(6/(1 + 4\Omega^2\tau^2) - 1)/r^6 \qquad (1)$$

where Ω is the Larmor frequency in rad·s^{-1} and r is the internuclear separation in angstrom units, which was taken to be 2.48 Å for ortho protons in the aromatic residues. Apparent correlation times were also estimated from cross-peak intensities in NOESY spectra recorded with a mixing time of 50 ms, by normalizing to the intensity of resolved diagonal peaks. This was done either as the two-spin approximation (Lane, 1989) or by calculating the average diagonal peak volume at a mixing time of zero using the selective T_1 value of the resolved diagonal peak (Mirau, 1988).

Circular Dichroism Measurements. CD spectra (near-UV, 330–255 nm; far-UV, 260–200 nm) were recorded at 22 °C with a Jasco J-600 spectropolarimeter. The instrument time constant was 0.5 s, and multiple scans were averaged. Near-UV spectra were recorded at a protein concentration of 5–6 mg/mL (300–360 μM) using fused silica cuvettes with a path length of 10 mm. Far-UV spectra were recorded at the same protein concentration using a demountable cuvette with a path length of 0.1 mm. The use of high protein concentrations for the far-UV measurements greatly reduces the problems of interference from extraneous calcium but does limit measurements to wavelengths greater than 200 nm. The reported spectra are presented in terms of molar ellipticity, based on a mean residue weight of 112.7. The standard buffer for the CD studies was 10 mM Tris·HCl, pH 7. Apo-CaM was prepared by gel filtration in 10 mM HCl on a PD-10 column. Secondary structure analysis was performed using the method of Provencher and Glockner (1981).

Time-Resolved Fluorescence Methods and Analysis. Fluorescence was excited at 285 nm using the frequency-doubled Coherent Antares laser system as described (Janot et al., 1991). Emission at 320 nm was isolated with an interference filter. Samples of calmodulin at 0.5 mg/mL in Tris or acetate buffers were in 10-mm path length cuvettes thermostated at 20 °C. Solutions contained either 1 mM Ca^{2+} or 1 mM EGTA; following the measurements, trifluoroethanol was added to 50% (v/v), and the measurement cycle was repeated. After the anisotropy measurement (up to 1 h), samples were examined by steady-state fluorescence to ensure the absence of photochemical modification [cf. Small & Anderson (1988)].

Time-resolved single photon counting data were collected at a frequency of 10 kHz with 19.92 ps/channel for 512 channels each for both V and H polarizations. Peak counts in the total decay ($V + 2H$) were in the range (7–9) × 10^{+4} and in the difference curve ($V - H$) 2 × 10^{+4}, whereas total counts were generally 5 × 10^{+6} and 1 × 10^{+6} for the sum and difference curves.

The analysis followed methods previously described (Janot et al., 1991) using a combination of linear regression and Marquardt fitting. Total intensity was measured either as the sum of $V + 2H$ or directly as the emission observed through a polarizer set at the magic angle. The initial analysis used a three-exponential fit to the total intensity data. It was generally found that a four-exponential fit was required in order to minimize χ^2 in the region of unity, to give appropriate values of the Durbin–Watson statistical parameter and to produce a normal distribution in the autocorrelation of residuals, devoid of systematic deviations. The shortest lifetime was then in the range 50–150 ps, and although it contributes only a few percent to the total intensity, it appears to be a significant component.

Analysis of the anisotropy decay was performed as described (Janot et al., 1991). The least-squares Marquardt fit was made simultaneously to the two observed polarization components, V and H, with appropriate weighting. Either a one-component or two-component exponential function was used for the anisotropy decay, and, in the latter case, all the cross terms between lifetimes and correlation times were included. Under all experimental solution conditions, it was found that a two-component function was required to give a minimized χ^2 close to unity. From the fitted parameters, amplitudes r_1 and r_2 and correlation times ϕ_1 and ϕ_2, the corresponding function for $r(t)$ was calculated as

$$r(t) = r_1 \exp(-t/\phi_1) + r_2 \exp(-t/\phi_2) \qquad (2)$$

On the "tumbling in a cone" hydrodynamic model (Kinosita et al., 1977), the values of r_1 and r_2 relate to α, the semiangle of the cone by

$$r_1/(r_1 + r_2) = 0.25[\cos^2\alpha(1 + \cos\alpha)^2] \qquad (3)$$

where $r_1 + r_2 = r(0)$, the initial anisotropy. This is usually equated with r_0, the intrinsic anisotropy measured for an immobilized chromophore in a rigid medium. For tyrosine model compounds, r_0 is given as 0.24–0.25 (Kilhoffer et al., 1981; Lambooy et al., 1982).

Interpreted as a single faster component, superimposed upon the slower global motion, the corresponding molecular correlation times are given as

$$1/\phi_f = 1/\phi_1 - 1/\phi_2 \quad \text{and} \quad \phi_s = \phi_2 \qquad (4)$$

Essentially the same values of the fitted parameters for a two-component anisotropy analysis were obtained for a given set of data, irrespective of whether the three- or the four-component lifetime fit to the total fluorescence intensity decay was used.

Results

Circular Dichroism Spectra. CD measurements were made to check that the integrity of calmodulin was unchanged after

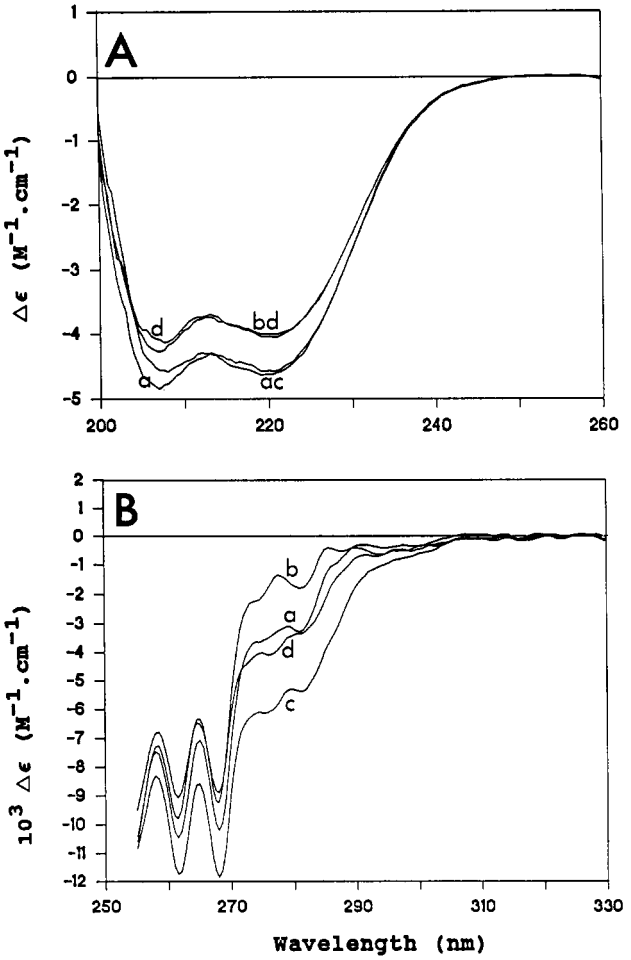

FIGURE 1: (A) Far-UV CD spectra: (a) apo-CaM at pH2; (b) apo-CaM adjusted from pH 2 to 7; (c) Ca_4–CaM at pH 7; and (d) EGTA–CaM generated at pH 7 by the addition of excess EGTA to Ca_4–CaM. (B) Near-UV CD spectra: (a) apo-CaM at pH2; (b) apo-CaM adjusted from pH 2 to 7; (c) Ca_4–CaM at pH 7; and (d) EGTA–CaM generated at pH 7 by the addition of excess EGTA to Ca_4–CaM.

pH 2 treatment (used in ensuring the complete removal of Ca^{2+}; see Materials and Methods) and to compare the properties of this apo-CaM with EGTA–CaM, as frequently used in physical studies. Figure 1A shows the effect of Ca^{2+} on the secondary structure of calmodulin. The total α-helical structure increases when Ca^{2+} binds to calmodulin; the far-UV CD of Ca_4–CaM (spectrum c) and EGTA-CaM (spectrum d) are very similar to those reported previously (Martin & Bayley, 1986). However, the far-UV CD of apo-CaM at pH 2 (spectrum a) is seen to be nearly identical to that of Ca_4–CaM at pH 7 (spectrum c) [cf. Bayley et al. (1988)]. The far-UV CD spectrum of apo-CaM on adjustment to pH 7 (spectrum b) is similar to that of EGTA–CaM (spectrum d), as expected. These results show that the low-pH treatment produces viable apo-CaM, as judged by the expected far-UV CD intensities and the changes on binding Ca^{2+}. Protonation of this apo-CaM at pH 2 gives a conformation with α-helical content close to that observed for Ca_4–CaM at pH 7.

In Figure 1B, comparison of spectra c and d shows that removal of Ca^{2+} by adding excess EGTA at pH 7 causes a significant but limited decrease in the near-UV CD, associated with Tyr-99 and Tyr-138 [cf. Martin and Bayley (1986)]. By contrast, the spectrum of apo-CaM after acid treatment and adjustment to pH 7 in the *absence* of Ca^{2+} (spectrum b) shows significantly lower CD intensity at wavelengths >270 nm compared with EGTA–CaM at pH 7 (spectrum d). However,

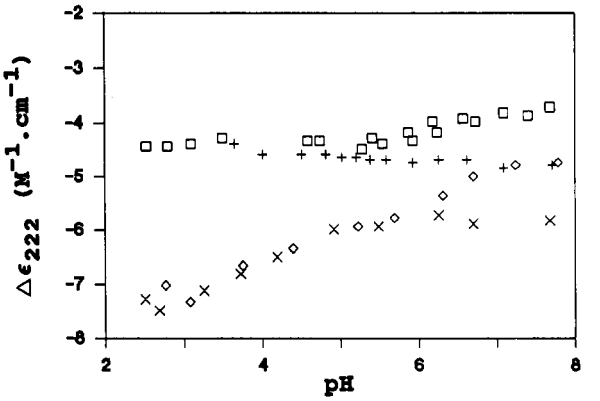

FIGURE 2: Far-UV CD intensity at 222 nm as a function of pH for Ca_4–CaM in aqueous buffer (+), Ca_4–CaM in 50% (v/v) trifluoroethanol (×), EGTA–CaM in aqueous buffer (□), and EGTA–CaM in 50% (v/v) trifluoroethanol (◇).

apo-CaM at pH 2 (spectrum a) shows a near-UV CD spectrum similar to that of EGTA–CaM at pH 7 (spectrum d).

Further experiments showed the following:

(1) Increasing the pH of a solution of EGTA–CaM from 7.0 to 9.0 (which increases the apparent affinity of EGTA for Ca^{2+} by >1000-fold) does not change the near-UV CD spectrum. Therefore, the CD intensity of curve d (Figure 1B) is unlikely to be due to the inability of EGTA to remove all the Ca^{2+} from calmodulin.

(2) Addition of stock Na_4-EGTA (5 mM; pH 7) to a solution of apo-CaM at pH 7 converted the near-UV CD spectrum from b to d, suggesting that some component in the EGTA solution, either EGTA itself or the counterion (Na^+), is responsible.

(3) Addition of Tris–EGTA (5 mM) to a solution of apo-CaM at pH 7 had no effect, whereas addition of NaCl (50 mM) again converted the near-UV CD spectrum from b to d. This confirms that binding Na^+ evidently affects the environment of aromatic residues.

The effect of pH changes on calmodulin conformation is shown in Figure 2. The far-UV CD intensity for Ca_4–CaM is almost constant from pH 7.7 to 4 (with slight decrease) and is very similar to that of EGTA–CaM at pH <5. Figure 1A showed the identity of α-helical content for Ca_4–CaM at pH 7 and apo-CaM at pH 2. This indicates that the α-helical composition is indeed the same throughout this pH range. More importantly, it suggests that Ca^{2+} can be replaced in binding to E-F hands by protons, with relatively little perturbation of the secondary structure. We note that mildly acidic partially nonaqueous crystallization conditions were used for determining the high-resolution crystal structures of calmodulin and troponin C (Babu et al., 1985; Herzberg & James, 1988; Satyshur et al., 1988).

In this work, and previous studies [summarized in Martin and Bayley (1986)], the α-helical content of Ca_4–CaM derived from the far-UV CD intensity by conventional procedures (see Materials and Methods) appears to be significantly less by some 10% than the 65–70% calculated from the crystal structure of Babu et al. (1985). However, there is some evidence of distorted α-helices in certain E-F hand structures [see Trewhella et al. (1989)]. In the high-resolution structure of carp parvalbumin at 1.9 Å (Kretsinger & Nockolds, 1973; Moews & Kretsinger, 1975), the conformation of several residues was reported to be intermediate between α-helix and the 3_{10}-helix. Theoretical calculations (Manning et al., 1988; Manning & Woody, 1991) show significant differences in the far-UV CD intensity for 3_{10} conformations, strongly dependent upon the parameters of the model structure. The 3_{10} con-

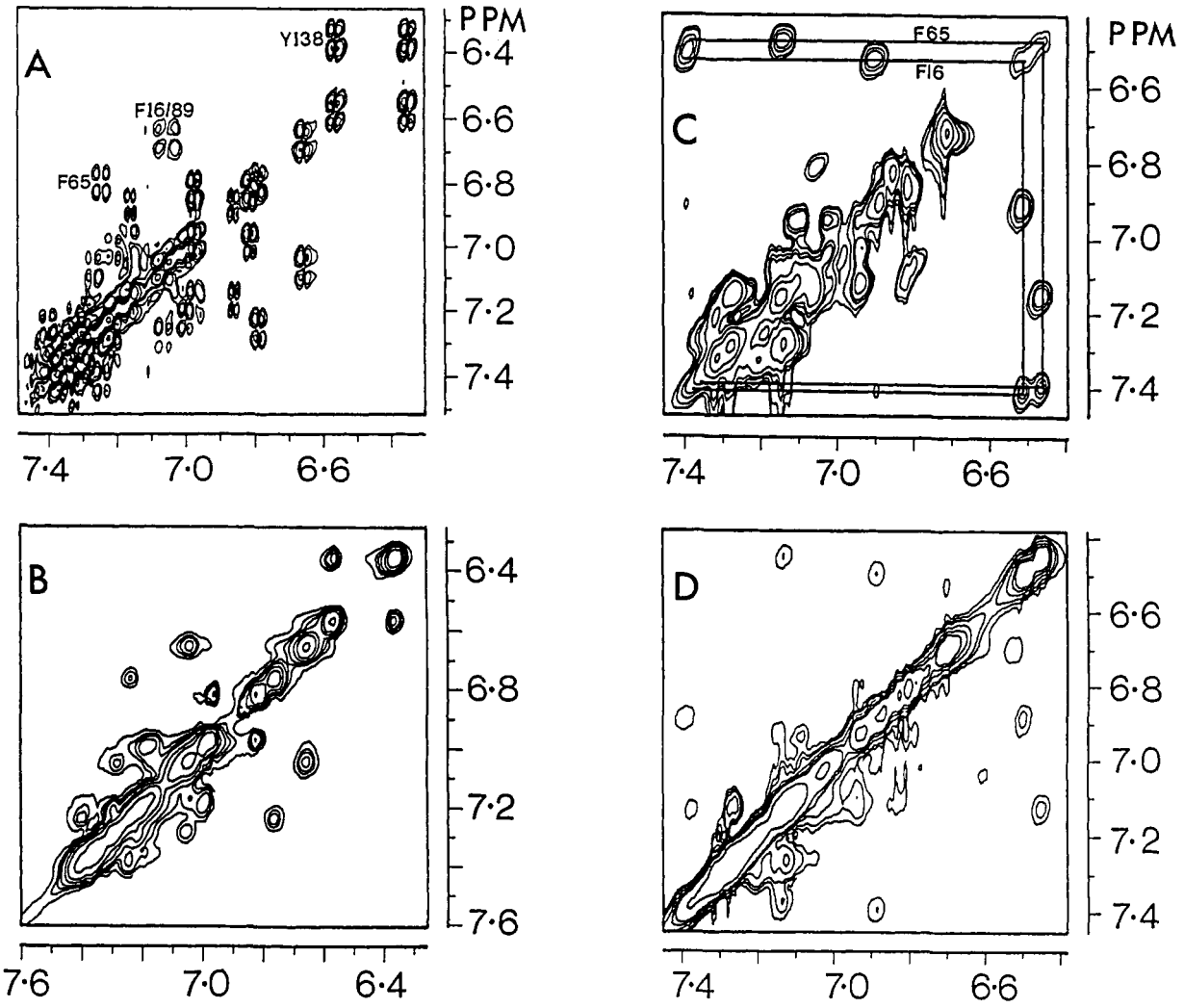

FIGURE 3: (A and B) NMR spectroscopy of Ca_4–CaM. (A) DQF-COSY spectrum and (B) NOESY spectrum (mixing time = 50 ms). Spectra were recorded at 40 °C as described under Materials and Methods. The free induction decays were apodized in both dimensions using a sine-squared function shifted by 60°. The digital resolution was 2.9 Hz per point in F_2 and 6 Hz per point in F_1 for the COSY spectrum and 1.7 Hz per point in F_2 and 3.4 Hz per point in F_1 for the NOESY spectrum. (C and D) NMR spectroscopy of apo-CaM. (C) HOHAHA spectrum (mixing time = 48 ms) and (D) NOESY spectrum (mixing time = 50 ms). Spectra were recorded at 40 °C as described under Materials and Methods. The free induction decays were apodized in both dimensions using a sine-squared function shifted by 60° (NOESY) or 45° (HOHAHA) in F_2, and by 60° in F_1 for both spectra. The digital resolution was 2.2 Hz per point in F_2 and 4.3 Hz per point in F_1.

formation is seen in alamethicin and peptides containing aminoisobutyric acid [see Nagaraj and Balaman (1981)], and these show attenuated far-UV CD. It thus appears possible that subtle effects, such as small changes in liganding at the Ca^{2+}-binding sites or environmental changes (e.g., helicogenic solvents), could affect the relative proportions of α- and 3_{10}-helix, producing changes in far-UV CD which could not be assigned unambiguously to a change in α-helical content.

The recent structure of carp parvalbumin at 1.5-Å resolution (Kumar et al., 1990) clarifies some of these questions for proteins containing E-F hands. Most of the helices previously thought to be distorted now appear more regular, but there is a small region of seven residues of 3_{10}-helix in helix D, which would be analogous to the F helix of sites I and III in calmodulin. A 100% decrease in the far-UV CD of 15 residues (out of 149 residues in calmodulin) would be required to reduce the apparent total α-helical content by 10%. Since this 100% attenuation represents the limit of the theoretical results, it appears unlikely that helix distortion toward the 3_{10} conformation could be exclusively responsible for the low intensity of far-UV CD seen in Ca_4–CaM. In addition, the poor definition of the central helix, as seen in the crystal structure of calmodulin (Babu et al., 1988), may be significant.

In this context, the sensitivity of calmodulin to changes in environment is directly relevant. The effect of the helicogenic solvent 50% TFE on the secondary structure of calmodulin is substantial at all pH values (Figure 2). At pH 7, as previously reported (Bayley et al., 1988), 50% TFE causes a marked increase in α-helical content in both Ca_4–CaM and EGTA–CaM. At pH 5.5 in 50% TFE, the far-UV CD intensities of Ca_4–CaM and EGTA–CaM are similar, and both undergo a further increase at pH <5 so that the highest α-helical content induced (>70% at pH 3, 50% TFE) is at least as great as that observed in the crystal structure. It appears likely that nonaqueous additives used in crystallization, such as 2-methyl-2,4-pentanediol (Cook & Sack, 1983), may induce additional α-helix, particularly at pH 5 (Bayley et al., 1988). We conclude that the α-helix content of Ca_4–CaM in aqueous solution is significantly less than estimated from the crystal structure. Treating the central region as a continuous α-helix tends to overestimate the calculated α-helical content of Ca_4–CaM relative to its conformation in aqueous solution.

NMR Spectra. Figure 3A,B shows the aromatic regions of the DQF-COSY and NOESY spectra of Ca_4–CaM at 40 °C. Assignments are taken from the literature (Ikura et al., 1983, 1984; Dalgarno et al., 1984; Seeholzer & Wand, 1989).

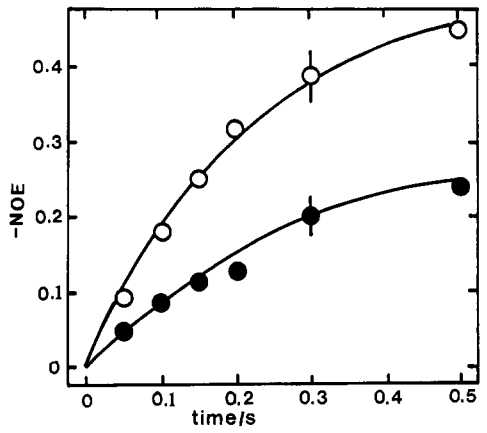

FIGURE 4: NOE buildup curves in Ca_4–CaM and apo-CaM. One-dimensional truncated NOE spectra were recorded at 40 °C as described under Materials and Methods. The continuous lines are least-squares regression fits to the appropriate two-spin equation. Y99, Ca_4-CaM (○); F16, apo-CaM (●).

The correspondence of the cross-peaks in the NOESY and COSY experiments shows that the NOESY cross-peaks are intraresidue. Even with a mixing time of 50 ms, the NOESY cross-peak intensities are relatively large, indicating that magnetization transfer is dominated by slow tumbling.

In contrast, the relative NOESY cross-peak intensities in apo-CaM are weaker than those in Ca_4–CaM, as shown in Figure 3C,D. Again, the NOESY cross-peaks arise from magnetization transfer within aromatic residues, as shown by the comparison of the NOESY and HOHAHA spectra. The NOESY cross-peak intensities indicate that the rate of magnetization transfer between neighboring protons within the aromatic residues in apo-Cam is substantially lower than in Ca_4–CaM. Because the proton–proton distances are all the same (2.47 Å), the lower rate of magnetization transfer in apo-CaM indicates that the correlation time for proton–proton vectors is smaller than for Ca_4–CaM. The resolution of the spectra is such that many of the desired cross-relaxation rate constants can be reliably determined using one-dimensional methods. In the more crowded region of the spectrum, between 7 and 7.5 ppm, it is not possible to excite individual resonances by selective irradiation, but the cross-peaks in the NOESY spectrum are sufficiently resolved to allow reliable volume integration. Figure 4 shows typical 1D NOE buildup curves at 40 °C, from which the cross-relaxation rate constants can be determined. The results are given in Table I.

The apparent rotational correlation times at 40 °C in the presence of Ca^{2+} vary from 6 to 10 ns; the values for Tyr-138 are smaller than those for Tyr-99 and for the Phe residues. This may reflect slight differences in internal motion or different alignment of the Tyr-99 vector relative to a molecular rotation axis. Nevertheless, the correlation times are all rather similar, with a mean of 8.9 ± 1.4 ns. A similar spread of values is found at 15 °C, where the mean correlation time is 17.9 ± 2.8 ns. Correcting these correlation times in ^2H_2O to 20 °C and H_2O gives a value of 12.0 ± 1.9 ns. However, the viscosity of the solutions used for NMR (≈50 mg of protein/mL) is ≈15% greater than for water, and this further correction gives 10.4 ± 1.6 ns.

The rotational correlation time for a spherical molecule of molecular mass M is given by the Stokes–Einstein equation:

$$\tau_R = \eta V/RT = M(v + h)\eta/RT \qquad (5)$$

For H_2O at T = 293 K, the viscosity η = 0.01 P; V is the hydrated volume, R is the gas constant, and v is the partial specific volume = 0.71 mL/g. For a typical degree of hydration (h = 0.3 g/g protein), a spherical protein of M = 16700 has τ_R = 6.9 ns (Cantor & Schimmel, 1980). The fact that observed correlation times are up to 1.5-fold greater is consistent with a significantly larger hydrodynamic volume. The ratio of the correlation times at 15 and 40 °C is 2.0, as expected from eq 5.

Table I: Correlation Times in Calmodulin Determined by NOE Spectroscopy[a]

		T = 40 °C		T = 15 °C		
proton pair	δ 1,2 (ppm)	$-\sigma$ (s^{-1})	τ (ns)	$-\sigma$ (s^{-1})	τ (ns)	method
Ca_4–CaM						
Y138 2-3	6.35, 6.55	1.54	6.1	3.7	14.4	1D
Y138 3-2		2.0	7.8	4.1	16.1	2D
Y99 2-3	6.80, 6.97	2.3	8.9	5.5	21.4	1D
Y99 2-3		2.1	8.2	nd	nd	2D
F16/89[b] 2-3	6.64, 7.05	1.6	6.2	5.0	19.7	1D
F16/89 2-3		2.2	8.7			2D
F16/89 3-2	7.05, 6.64	2.1	8.1			2D
F16/89 3-4	7.05, 7.28	2.5	9.8			2D
F65 2-3	6.76, 7.23	nd				1D
F65 3-2	7.23, 6.76	nd				1D
F65 3-4	7.23, 7.39	nd				1D
F65 2-3		2.4	9.4			2D
F65 3-4	7.00, 7.20	2.5	9.8			2D
apo-CaM						
F65 2-3	6.46, 7.13	1.06	4.4	3.0	11.6	ND
F65 2-3		1.04	4.2	nd	nd	2D
F65 3-2		nd	nd	2.7	10.6	1D
F65 3-4	7.13, 7.17	nd	nd	2.2	8.7	1D
F16 2-3	6.51, 6.89	1.0	4.1	2.4	9.4	1D
F16 3-2		1.1	4.5	2.5	9.8	1D
F16 3-4	6.78, 7.41	1.1	4.5	2.7	10.6	1D

[a] Resonance assignments were taken from the literature as described in the text. Correlation times were determined from NOESY and truncated one-dimensional NOE experiments as described in the text. Probable error on individual τ = ±15%; 1D, truncated one-dimensional NOE; 2D, NOESY. Shifts were measured at 40 °C. [b] Two resonances under this peak.

For apo-CaM, the correlation times are substantially smaller than for Ca_4–CaM and are more closely similar for aromatic residues found in different parts of the molecule. Again, the temperature dependence of the rotational correlation times is consistent with the Stokes–Einstein law. Converting the measured values to standard 20 °C, H_2O, with correction for protein viscosity gives a mean correlation time of 6.0 ± 0.5 ns. This smaller value indicates either that apo-CaM is more spherical or that there is a substantial increase in segmental motion affecting all the observed residues.

The measured correlation times always represent lower limits on the rotational correlation time of the molecule as a whole, because internal motions about axes other than the C_β–C_γ bond will decrease the measured cross-relaxation rate constant. Fast (<1 ns) internal motions are not resolved in these NOE measurements. Although both the CD data and the measured correlation times strongly indicate significant changes in both conformation and dynamics, it is clear from the CD that apocalmodulin retains the major elements of its secondary structure. This is supported by the NOESY spectrum of apo-CaM in ^1H_2O (A. N. Lane, unpublished work). This spectrum shows the presence of amide protons resonating above 9 ppm, αCH resonating above 5 ppm, $d_{\alpha N}$ connectivities typical of the antiparallel β-sheet, and extensive d_{NN} connectivities and αCH shifts bunched together near 4 ppm, typical of the α-helix conformation (Szilagyi & Jardetzky, 1989). Upfield-shifted methyl resonances are also consistent with substantial tertiary structure interactions, which are further supported by chemical shifts of the aromatic resonances different from the random-coil values.

Table II: Parameters of Time-Resolved Fluorescence and Associated Anisotropy Analysis for One and Two Correlation Times[a]

conditions	lifetime τ (ps)						anisotropy: correlation time ϕ (ps)						
($\pm Ca^{2+}$, pH)	$n = 1$	$n = 2$	$n = 3$	$n = 4$	χ^2	DW	i	ϕ_1	r_1	ϕ_2	r_2	χ^2	DW
$+Ca^{2+}$, 7.08													
τ	50	352	1341	3222	0.98	1.90	1	6276	0.215			1.50	1.34
sd	4	9	13	34			sd	62					
%	2	13	36	49			2	661	0.050	8740	0.184	0.99	2.06
							sd	64		269			
$+Ca^{2+}$, 4.60													
τ	67	412	1463	3269	0.99	1.93	1	9657	0.231			1.33	1.61
sd	5	10	29	37			sd	54					
%	2	12	35	51			2	651	0.038	12512	0.210	1.07	2.01
							sd	91		428			
$-Ca^{2+}$, 7.08													
τ	75	354	1052	3518	1.18	1.80	1	3632	0.210			3.71	0.55
sd	3	8	27	61			sd	31					
%	5	30	38	27			2	595	0.117	11031	0.131	1.13	1.80
							sd	25		653			
$-Ca^{2+}$, 4.60													
τ	150	488	1879	4507	1.09	2.03	1	8107	0.223			1.36	1.58
sd	9	17	80	357			sd	108					
%	6	22	52	20			2	543	0.045	10673	0.200	1.03	2.08
							sd	65		330			

[a] sd, standard deviation; %, fluorescence yield of the ith decay; DW, Durbin–Watson parameter.

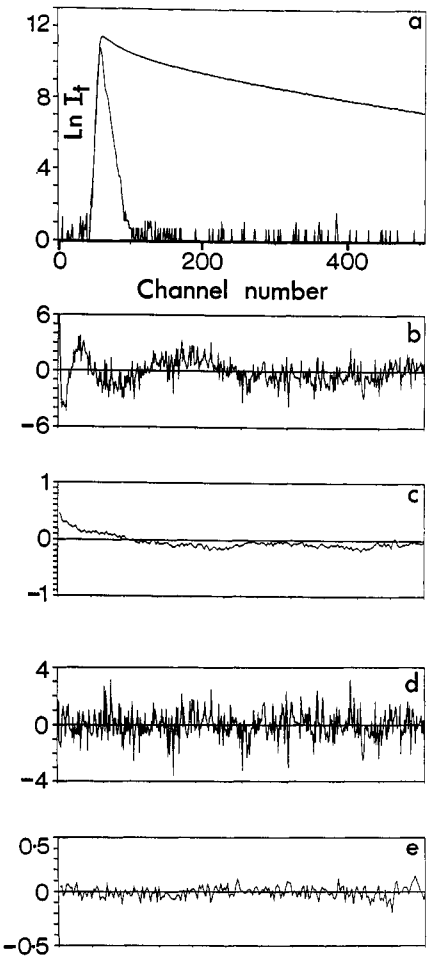

FIGURE 5: Analysis of time-resolved fluorescence decay of Ca_4–CaM at pH 7.0. Time per channel = 20 ps. Numerical data are given in Table II. (a) Intensity decay on natural logarithmic scale. (b) Residuals for three component fit (0–8.8 ns). (c) Autocorrelation function of residuals for the three-component fit in panel b (0–4.4 ns). (d) Residuals for the four-component fit (0–8.8ns). (e) Autocorrelation function of residuals for the four-component fit in panel d (0–4.4 ns).

Time-Resolved Fluorescence Measurements. The measurement of time-resolved fluorescence anisotropy of tyrosine residues has a number of intrinsic photophysical limitations, namely, the low quantum yield, the short lifetime, and the necessity for UV excitation in the range 280–285 nm. In previous work on calmodulin (Bayley et al., 1988), a synchrotron source was used. However, the pulse width was large and the total fluorescence counts were relatively low, thus imposing limitations on the resolution of short lifetime components and on assignment of longer correlation times. In reexamining the fluorescence decay of calmodulin in this work, advantage was taken of the improved performance of the pulsed laser system previously described (Janot et al., 1991). This source provides a high repetition rate with a pulse width (FWHM) ≈80 ps with high intensity at 285 nm. Thus, good time resolution and high total fluorescence counts, essential for anisotropy measurement, are readily achieved.

The fluorescence decay of tyrosine emission in calmodulin in the presence of 1 mM Ca^{2+} at pH 7.0 is shown in Figure 5. The superiority of the four-component fit is readily seen in the autocorrelation of residuals. The fluorescence decay was measured over ≈9 ns with the channel width routinely 20 ps. The corresponding fitting of the fluorescence anisotropy is shown in Figure 6. Using the four-component lifetime fit to the total intensity decay as in Figure 5, χ^2 is minimized for the two experimental curves V and H (treated globally) by refinement of parameters r_i and ϕ_i; the quality of fit is illustrated by comparing the experimental curve $(V - H)/(V + 2H)$ with that calculated from the derived anisotropy parameters. It is seen in Figure 6A that the one-component fit to the anisotropy (ϕ = 6276 ± 62 ps) is poor (χ^2 = 1.5); the two-component fit (ϕ_1 = 661 ± 64 ps, ϕ_2 = 8740 ± 269 ps) gives χ^2 = 0.99. The anisotropy parameters obtained at pH 7 for the single-exponential fit agree with those reported from previous work (Bayley et al., 1988). However, the improved data indicate the validity of the more complex solution with two correlation times at both pH 7.0 and 4.6.

Table II reports the analytical results for typical data for calmodulin under different conditions; the anisotropy results are shown for both one and two correlation times, the latter being obtained as a free fit of the four parameters r_1, ϕ_1, r_2, and ϕ_2. Table II shows that adjustment to pH 4.6 in the presence of 1 mM Ca^{2+} has virtually no effect on the lifetimes. The anisotropy, however, shows a marked change; the average

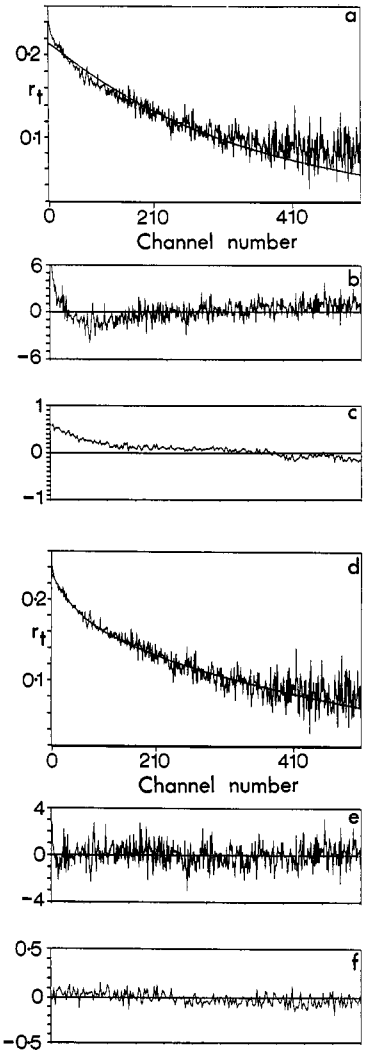

FIGURE 6: Analysis of time-resolved fluorescence anisotropy of Ca_4–CaM at pH 7.0 using (a–c) one and (d–f) two correlation times. (a and d) Anisotropy decay (linear scale): $r(t)$ derived from the experimental V and H plus (smooth line) the computed best fit using parameters from Table II and eq 2. (b and e) Residuals of $r(t)$ and the computed best fit (0–8.8 ns). (c and f) Autocorrelation function of residuals in (b and e) (0–4.4 ns).

value of the correlation time (given by $i = 1$) increases to more than 9 ns, and the two-component analysis shows correlation times of 650 and 12 500 ps with the major contribution to total anisotropy in the slower global rotation. On the Kinosita model (eq 3) the cone half-angle α has decreased from 23° (pH 7.0) to 19° (pH 4.6). Table II shows that removal of Ca^{2+} in the presence of 1 mM EGTA causes marked changes in both lifetime and anisotropy behavior at both pH values. EGTA–CaM at pH 7 shows a marked drop in mean correlation time to 3.6 ns. The two-component analysis gives only a marginally acceptable fit at $\chi^2 = 1.13$, suggesting this model is barely adequate to describe the dynamic properties. At pH 4.5, EGTA–CaM shows significant changes in lifetime and amplitudes of the two longer components. Under these conditions, the mean correlation time is 8 ns (i.e., greatly increased relative to the value at pH 7.0), and the anisotropy decay analyses have two components.

Figure 7 compares the calculated anisotropy decays for typical cases from Table II. It is seen that the two-component fits are significantly different from the one-component fits, and indeed from each other. On a segmental-motion model (eq 3), and correcting as per eq 4, the faster component appears consistently in the range of 500–600 ps for both Ca^{2+}

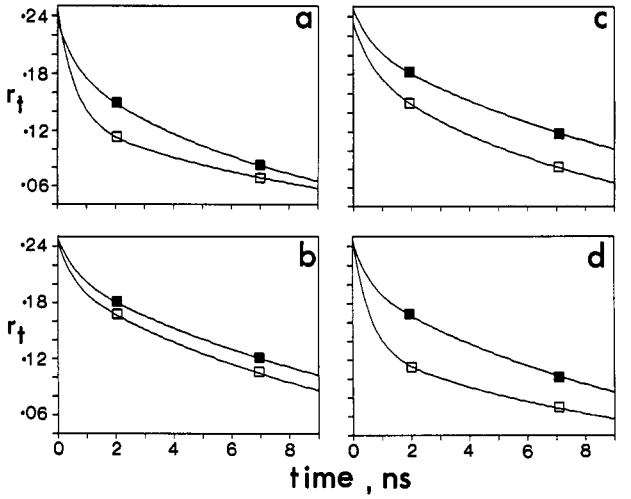

FIGURE 7: Comparison of computed best fits for two-component anisotropy decay functions; $r(t)$ calculated using the anisotropy parameters of Table II and eq 2. (Left) (a) Comparison of Ca_4–CaM (■) with EGTA–CaM (□) at pH 7.0 and (b) at pH 4.6. (Right) (c) Comparison of Ca_4–CaM at pH 7.0 (□) with Ca_4–CaM at pH 4.6 (■) and (d) comparison of EGTA–CaM at pH 7.0 (□) with EGTA–CaM at pH 4.6 (■).

Table III: Limits of the Anisotropy Analysis[a]

	ϕ_1	r_1	ϕ_2	r_2	χ^2
pH 7.0	0.64	0.050	8.65	0.185	0.99 (min)
	[0.64]	0.066	10.7	0.173	1.09
	[0.64]	0.030	7.1	0.198	1.10
	0.30	0.057	[8.65]	0.190	1.10
	1.40	0.049	[8.65]	0.175	1.10
pH 4.6	0.65	0.038	12.5	0.211	1.07 (min)
	[0.65]	0.018	10.0	0.224	1.18
	[0.65]	0.057	16.5	0.199	1.18
	2.30	0.038	[12.5]	0.199	1.18
	0.18	0.059	[12.5]	0.217	1.18

[a] Obtained by using data for Ca_4–CaM, at pH 7.0 and 4.6; the table shows the range of values of (ϕ_i, r_i) giving fits within the range $\chi^2_{(min)} \pm 10\%$.

and EGTA conditions. This value appears significantly longer than expected for a freely rotating label attached to a protein of this size, which could be <100 ps. It thus appears reasonable to associate it with a segmental motion of that part of calmodulin containing the tyrosine fluorophores. The two tyrosine residues of bovine brain calmodulin (Y99 and Y138) are involved in Ca^{2+}-binding sites III and IV, which together comprise the C-terminal half of the molecule.

The absolute values of these correlation times are reported with the analytical standard deviations. As has been well documented (Press et al., 1986), such solutions are often degenerate; a different estimate of the possible range is obtained by analyses in which one correlation time is fixed, and r_1 and r_2 plus the other correlation time are taken as variables. A typical result (for the pH 7.0 data set for Ca_4–CaM) shows that fits with χ^2 up to 10% above the minimum (i.e., $\chi^2 < 1.10$) are included in the ranges $\phi_1 = 0.3$–1.4 ns with $\phi_2 = 8.65$ ns and conversely $\phi_2 = 8.6$–10.7 ns for $\phi_1 = 0.64$ ns (see Table III). Thus, for comparative purposes, mean correlation times may be more useful. For Ca_4–CaM, the mean anisotropy increases monotonically from pH 7.0 to 4.6. A similar trend is shown by EGTA–CaM, although the values are generally lower, and it clearly has a more dynamic state at pH 7.0. In the presence of 50% TFE, when the α-helical content of both Ca_4–CaM and EGTA–CaM is significantly increased (Bayley et al., 1988; Figure 2), the total intensity decay is well fitted with four lifetime components (data not shown) and always

requires more than one correlation time to describe the anisotropy properties. The apolar solvent increases the proportions of longer lifetime components and, overall, leads to a decrease in the steady-state polarization [cf. Bayley et al. (1988)]. The presence of 50% TFE appears to prevent the increased correlation time at lower pH values, particularly for Ca_4–CaM.

Discussion

The Conformation of Apo-CaM and Ca_4–CaM. In the course of this work, it became apparent that different methods of preparing Ca-free calmodulin may result in different conformational properties. Treatment with EGTA or lowering the pH removes Ca^{2+} and reduces the α-helical content to a similar degree. However, depending on the counterion present in the EGTA solution, near-UV CD properties show that the local environment of the tyrosine residues may differ. Some caution is therefore indicated in the use of Na-EGTA to remove Ca^{2+} from calmodulin, since Na^+ appears to bind to apocalmodulin. Addition of up to 0.1 M NaCl (or KCl) was reported (Kilhoffer et al., 1981) to quench the tyrosine fluorescence of apocalmodulin, in contrast to the binding of Ca^{2+}, which produces a large fluorescence increase. However, unlike Ca^{2+} or protonation, Na^+ induces no detectable change in secondary structure (Figure 1A). Compared with Ca^{2+}, Na^+ binds very weakly and with different coordination. The induction of α-helical structure by Ca^{2+} may be coupled to formation of the typical 7-coordinated Ca^{2+} in the E-F hand binding site. It is possible that protonation could bridge an empty site by promoting hydrogen bonding between the carboxylates, the principal charged ligands of the E-F hand. This would suggest that the conformational change to lower α-helix results when the negative charge density of the calcium-binding sites is not (at least partially) compensated by tight bivalent ion binding or by protonation. The highly conserved bidentate glutamate ligand at position 12 in the loop sequence has been shown by mutagenesis to be essential for normal calcium affinity (Maune et al., 1992) and for maintaining kinetic and conformational properties in the presence of Ca^{2+} (S. R. Martin, J. M. Maune, K. Beckingham, P. M. Bayley, manuscript in preparation). It is therefore possible that this bidentate property is functionally important in bringing the two sides of the loop together.

Properties of the Tyrosine Fluorophore. Time-resolved properties of the intrinsic tyrosine fluorophores report directly on the dynamics of specific areas within calmodulin itself. The data of Table II show there is a fast process involving the tyrosine residues of calmodulin with a correlation time $\approx$600 ps. This is present in apo-CaM and, to a lesser extent, in Ca_4–CaM at pH 7 and 4.5. Several reports note that removal of Ca^{2+} from calmodulin increases the tyrosine dynamics at pH 7 [cf. Bayley et al. (1988), Small and Anderson (1988), Wang et al. (1988), and Gryczynski et al. (1988, 1991)]. In the crystal structure of Ca_4–CaM, Tyr-99 appears to be partially accessible to solvent and faces into site III, whereas Tyr-138 points away from site IV and is in a hydrophobic loop. Sequences close to both tyrosines are involved in the β-sheet structure between sites III and IV (Babu et al., 1985, 1988). Tyr-99 is reported to have a 2.3-fold higher quantum yield compared to Tyr-138 (Kilhoffer et al., 1981). The observation of the fast process indicates that significant side-chain motion occurs close to sites III and IV of Ca_4–CaM and that this is reduced but not eliminated when sites III and IV bind Ca^{+2}.

The two-component analysis of fluorescence anisotropy of Ca_4–CaM at pH 7 gives a global rotational correlation time of 8.6 ns, with a range (Table III) from 7 to 10 ns. For Ca_4–CaM in which the two tyrosines are photo-cross-linked, Small and Anderson (1988) observed a single correlation time of 9 ns, i.e., without a faster correlation time. This suggests that the local motion inferred from the present results is fully inhibited when the two tyrosines are cross-linked. This modification, which is entirely within the C-terminal domain, requires closer proximity of the two tyrosines than is found in the crystal structure and may involve additional conformation changes since there is a marked decrease in the calcium affinity. Their value of 9 ns for the cross-linked molecule was interpreted as indicating an axial ratio of 2.5 to 3. The absence of other correlation times predicted by theory (Rigler & Ehrenberg, 1973) for such a prolate ellipsoid was rationalized in terms of an essentially rigid structure, with specific orientation of the emission vector of the cross-linked fluorophore relative to the long axis. This interpretation now appears inconsistent with the indications of flexibility within the central region of the molecule (Persechini & Kretsinger, 1988a,b; Heidorn & Trewhella, 1988; Ikura et al., 1991a,b). Whereas simulations of rigid dumbbell structures have been made (de la Torre & Bloomfield, 1977a,b), the possibility of such flexibility introduces a new and unexplored class of hydrodynamic models. It is likely that such a flexible structure would have properties significantly different from the rigid dumbbell and might account for the observed single long rotational correlation time observed in this work and that of Small and Anderson (1988).

It is significant that the increased fluorescence anisotropy for Ca_4–CaM in acidic solution occurs under conditions which produce little change in the α-helical content (see Figure 2). This suggests an increase in the time-average separation of the domains. These results are consistent with those of Wang (1989), who used fluorescence energy transfer to detect a change to a more extended conformation between pH 7 and 5. Similar effects were found for troponin C (Wang et al., 1987), which shows pH-dependent conformational changes (Lehrer & Leavis, 1975). Other indications of a slower global correlation time for calmodulin at lower pH are seen in results of Steiner and Norris (1987) and Wang et al. (1988).

Comparison of Dynamic Observations by NMR and Fluorescence. Both techniques have intrinsic limitations which become apparent when the independent results of each are compared. The quality of the analysis of the time-resolved fluorescence anisotropy is limited by the finite lifetime of the fluorophore. Although multiple correlation times are clearly detectable, the estimated values necessarily carry rather large errors. By contrast, the NOE methods used here give a lower limit to the rotational correlation time, since the observed values will be shortened by internal motions.

Nonetheless, the estimation of the global correlation time of Ca_4–CaM in the range 9–12 ns by either method is significantly greater than the value of 7 ns expected for a spherical molecule, indicating a more complex hydrodynamic behavior. Further, the variation in values of the rotational correlation time for residues in different parts of the molecule (Table I) would be consistent with a significant degree of overall molecular asymmetry, though differential internal mobility could also contribute to this range.

The global rotational correlation times reported here compare well with measurements of the radius of gyration from small-angle X-ray scattering (Heidorn & Trewhella, 1988), which indicate that calmodulin undergoes a small but significant change in hydrodynamic shape on the addition of Ca^{2+}. The far-UV CD of both calmodulin and its tryptic fragments show significantly increased α-helix in the presence

of Ca^{2+}, with the greater effects observed for the C-terminal domain (Martin & Bayley, 1986). NMR data suggest that the local environment of the Ca^{2+}-binding sites changes, with increased hydrogen-bond strengths in the β-strand loops of the E-F hands (Ikura et al., 1985, 1987) but not involving major changes in three-dimensional structure. In the absence of Ca^{2+} and at pH 7, the observed correlation times for residues in both the structural domains of calmodulin are lower, apparently conforming closer to that for a spherical hydrodynamic volume. However, the radius of gyration changes relatively little (Heidorn & Trewhella, 1988) so that the decrease is more likely due to increased internal mobility, consistent with the greater amplitude of the fast process in fluorescence anisotropy for apo-CaM.

The effect of fast internal motion on the correlation times deduced from the NMR studies has been treated quantitatively by Lipari and Szabo (1982). Ignoring the relatively small effect of rotational anisotropy, the cross-relaxation rate constant observed in the presence of fast internal motion is given by

$$\sigma(\text{obs}) = (1 - S^2)\sigma(\tau_e) + S^2\sigma(\tau_c)$$

where τ_e is a composite correlation constant defined as

$$\tau_e = \tau_c\tau_i/(\tau_c + \tau_i)$$

where τ_c is the global correlation time, τ_i is the correlation time for internal motion, and S^2 is the order parameter. When $\tau_c \gg \tau_i$, $\tau_e \approx \tau_i$. For $\tau_e = 0.5$ ns, from eq 1, $\sigma(\tau_e) = 0.056$ s^{-1}, compared with $\sigma(\tau_c) = 3$ s^{-1} for $\tau_c = 12$ ns. Hence, unless S^2 is smaller than ≈ 0.05, the ratio of the observed cross-relaxation rate constant for apo-CaM to that of Ca_4–CaM gives a reasonable estimate of the order parameter S^2 for residues in the N-terminal domain of apo-CaM. From the mean values, $S^2 = 0.55$. In the presence of calcium, from the fluorescence data of Table II, for the tyrosine residues of the C-terminal domain, the mean value of $S^2 = r_2/(r_1 + r_2) = 0.53$. These numbers are clearly similar. For motion within a cone (eq 3), this value would correspond to a cone semiangle of 35°. We note that this mobility not only occurs on the subnanosecond time scale but also requires motions about bonds other than $C_\beta C_\gamma$. Hence the NMR data and the fluorescence data, taken together, indicate that the internal mobility is not confined to the C-terminal domain, suggesting that the complete removal of calcium results in a widespread increase in dynamics of aromatic side chains in the calmodulin structure. This flexibility suggests that, especially for apo-CaM, a unique conformation may not exist, rendering conformational analysis unusually difficult.

Allowing for the different sensitivity of the NMR and optical parameters to internal motion, the results are consistent with an extended, and environmentally sensitive, flexible overall shape for Ca_4–CaM in solution. Ca_4–CaM is evidently less extended in solution than indicated by the crystal structure but apparently becomes more extended at lower pH. The sensitivity of calmodulin to local environment may be important in its biological function. It is now known from NMR studies (Ikura et al., 1991a,b) that the central sequence of calmodulin is not a permanent, continuous α-helix, consistent with the flexibility deduced from cross-linking studies (Persechini & Kretsinger, 1988). Further, peptides derived from calmodulin target sequences derived from MLCK and phosphorylase kinase cause major and specific changes in the global conformation of Ca_4–CaM without apparently affecting the conformations of the Ca^{2+}-bound domains themselves (Seeholzer & Wand, 1989; Heidorn et al., 1989; Trewhella et al., 1990). However, Ikura et al. (1991b) show that binding the MLCK peptide M-13 causes extensive changes in Ca_4–CaM conformation. These are most pronounced in the central region, with additional dynamic effects in the peptide NH exchange of the E helix of site I, the F helix of site III, and the F helix of site IV. The present work suggests that the aromatic residues in both N-terminal and C-terminal domains may provide useful complementary information on the specificity and dynamic structure of complexes of calmodulin with target peptide sequences.

Acknowledgments

We thank Dr. D. R. Trentham for constructive suggestions and for support and Drs. M. Ikura, L. Kay, and A. Bax for communicating data prior to publication. We acknowledge the assistance of Prof. D. Phillips and Dr. A. Beeby, Royal Institution, London, and Imperial College, London, for fluorescence decay measurements, and Mr. Keith M. Fairhall, for atomic absorption measurements.

Registry No. Ca^{2+}, 7440-70-2; H^+, 12408-02-5.

References

Aulabaugh, A., Niemczura, W. P., Blundell, T. L., & Gibbons, W. A. (1984) *Eur. J. Biochem. 143*, 409–418.

Babu, Y. S., Sack, J. S., Greenhough, T. J., Bugg, C. E., Means, A. R., & Cook, W. J. (1985) *Nature 315*, 37–40.

Babu, Y. S., Bugg, C. E., & Cook, W. J. (1988) *J. Mol. Biol. 204*, 191–204.

Bax, A., & Davis, D. G. (1985) *J. Magn. Reson. 65*, 355–360.

Bayley, P. M., Martin, S. R., & Jones, G. (1988) *FEBS Lett. 238*, 61–66.

Cantor, C. R., & Schimmel, P. R. (1980) *Biophysical Chemistry*, p 461, W. H. Freeman and Co., San Francisco, CA.

Cook, W. J., & Sack, J. S. (1983) *Methods Enzymol. 102*, 143–147.

Dalgarno, D. C., Klevitt, R. E., Levine, B. A., Williams, R. J. P., Dobrowolski, W., & Drabikowski, W. (1984) *Eur. J. Biochem. 138*, 281–289.

De la Torre, J. G., & Bloomfield, V. A. (1977a) *Biopolymers 16*, 1747–1763.

De la Torre, J. G., & Bloomfield, V. A. (1977b) *Biopolymers 16*, 1765–1778.

Dobson, C. M., Olejnicjak, E. T., Poulsen, F. M., & Ratcliffe, R. G. (1982) *J. Magn. Reson. 48*, 97–102.

Frankiel, T., Bauer, C., Carr, M. D., Birdsall, B., & Feeney, J. (1990) *J. Magn. Reson. 90*, 420–425.

Gopalakrishna, R., & Anderson, W. B. (1982) *Biochem. Biophys. Res. Commun. 104*, 830–836.

Gryczynski, I., Steiner, R. F., & Lakowicz, J. R. (1988) *Biophys. Chem. 30*, 49–59.

Gryczynski, I., Steiner, R. F., & Lakowicz, J. R. (1991) *Biophys. Chem. 39*, 69–78.

Haiech, J., Klee, C. B., & Demaille, J. D. (1981) *Biochemistry 20*, 3890–3897.

Hennessey, J. P., Manavalan, P., Johnson, W. C., Malencik, D. A., Anderson, S. R., Schimerlik, M. I., & Shalatin, Y. (1987) *Biopolymers 26*, 561–571.

Heidorn, D. B., & Trewhella, J. (1988) *Biochemistry 27*, 909–915.

Heidorn, D. B., Seeger, P. A., Rokop, S. E., Blumenthal, D. K., Means, A. R., Crespi, H., & Trewhella, J. (1989) *Biochemistry 28*, 6757–6764.

Herzberg, O., & James, M. N. G. (1988) *J. Mol. Biol. 203*, 761–779.

Ikura, M., Hiraoki, T., Hikichi, K., Mikuni, T., Yazawa, M., & Yagi, K. (1983a) *Biochemistry 22*, 2568–2572.
Ikura, M., Hiraoki, T., Hikichi, K., Mikuni, T., Yazawa, M., & Yagi, K. (1983b) *Biochemistry 22*, 2573–2579.
Ikura, M., Hiraoki, T., Hikichi, K., Minowa, O., Yamaguchi, H., Yazawa, M., & Yagi, K. (1984) *Biochemistry 23*, 3124–3128.
Ikura, M., Minowa, O., & Hikichi, K. (1985) *Biochemistry 24*, 4264–4269.
Ikura, M., Minowa, O., Yazawa, M., Yagi, K., & Hikichi, K. (1987) *FEBS Lett. 219*, 17–21.
Ikura, M., Kay, L. E., & Bax, A. (1990) *Biochemistry 29*, 4659–4667.
Ikura, M., Barbeto, G., Clore, M., Gronenborn, A., Kay, L., Spera, S., Zhu, G., & Bax, A. (1991a) *Biophys. J. 59*, 1a.
Ikura, M., Kay, L. E., Krinks, M., & Bax, A. (1991b) *Biochemistry 30*, 5498–5504.
Janot, J. M., Beeby, A., Bayley, P. M., & Phillips, D. (1991) *Biophys. Chem. 41*, 277–287.
Kataoka, M., Head, J. F., Seaton, B. A., & Engelman, D. M. (1989) *Proc. Natl. Acad. Sci. U.S.A. 86*, 6944–6948.
Kilhoffer, M. C., Demaille, J. G., & Gerard, D. (1981) *Biochemistry 20*, 4407–4414.
Kinosita, K., Kawato, S., & Ikegami, A. (1977) *Biophys. J. 20*, 289–305.
Klee, C. B. (1977) *Biochemistry 16*, 1017–1024.
Klee, C. B. (1980) in *Calcium and Cell Function* (Cheung, W. Y., Ed.) Vol. 1, Chapter 4, Academic Press, New York.
Klee, C. B. (1988) in *Calmodulin* (Cohen, P., & Klee, C. B., Eds.) Chapter 3, Elsevier, Amsterdam.
Klevitt, R. E., Dalgarno, D. C., Levine, B. A., & Williams, R. J. P. (1984) *Eur. J. Biochem. 139*, 109–114.
Kretsinger, R. H., & Nockolds, C. E. (1973) *J. Biol. Chem. 248*, 3313–3326.
Kretsinger, R. H., Rudnick, S. E., & Weissman, L. J. (1986) *J. Inorg. Biochem. 28*, 289–302.
Kumar, V. D., Lee, L., & Edwards, B. F. P. (1990) *Biochemistry 29*, 1404–1412.
Lane, A. N. (1989) *Eur. J. Biochem. 182*, 95–104.
Lane, A. N., Lefevre, J.-F., & Jardetzky, O. (1986) *J. Magn. Reson. 66*, 201–218.
Lambooy, P. K., Steiner, R. F., & Sternberg, H. (1982) *Arch. Biochem. Biophys. 217*, 517–528.
Lehrer, S. S., & Leavis, P. C. (1974) *Biochem. Biophys. Res. Commun. 58*, 159–165.
Lipari, G., & Szabo, A. (1982) *J. Am. Chem. Soc. 104*, 4546–4558.
Manning, M. C., & Woody, R. W. (1991) *Biopolymers 31*, 569–586.
Manning, M. C., Illangasekare, M., & Woody, R. W. (1988) *Biophys. Chem. 31*, 77–86.
Marion, D., & Wüthrich, K. (1983) *Biochem. Biophys. Res. Commun. 124*, 774–783.
Martin, S. R., & Bayley, P. M. (1986) *Biochem. J. 238*, 485–490.
Martin, S. R., Teleman, A. A., Bayley, P. M., Drakenberg, T., & Forsen, S. (1985) *Eur. J. Biochem. 151*, 543–550.
Martin, S. R., Linse, S., Bayley, P. M., & Forsen, S. (1986) *Eur. J. Biochem. 161*, 595–601.
Matsushima, N., Izumi, Y., Matsuo, T., Yoshino, H., Ueki, T., & Miyake, Y. (1989) *J. Biochem. (Tokyo) 105*, 883–887.
Maune, J. M., Klee, C. B., & Beckingham, K. (1992) *J. Biol. Chem.* (in press).
Mirau, P. (1988) *J. Magn. Reson. 80*, 439–447.
Moews, P. C., & Kretsinger, R. H. (1975) *J. Mol. Biol. 91*, 201–228.
Nagaraj, R., & Balaram, P. (1981) *Acc. Chem. Res. 14*, 356–362.
Newton, D. L., Oldewurtel, M. D., Krinks, M. H., Shiloach, J., & Klee, C. B. (1984) *J. Biol. Chem. 259*, 4419–4426.
O'Neil, K. T., & Degrado, W. F. (1990) *Trends Biochem. Sci. 15*, 59–64.
O'Neil, K. T., Erickson-Viitanen, S., & Degrado, W. F. (1989) *J. Biol. Chem. 264*, 14571–14578.
Persechini, A., & Kretsinger, R. H. (1988a) *J. Biol. Chem. 263*, 12175–12178.
Persechini, A., & Kretsinger, R. H. (1988b) *J. Cardiovasc. Pharmacol. 12, Suppl. 5*, S1–S12.
Press, W. H., Flannery, B. P., Teukolsky, S. A., & Vetterling, W. T. (1986) *Numerical recipes: the art of scientific computing*, Chapter 10, Cambridge University Press, Cambridge, U.K.
Provencher, S. W., & Glockner, J. (1981) *Biochemistry 20*, 33–37.
Ribeiro, A., Parello, J., & Jardetzky, O. (1984) *Prog. Biophys. Mol. Biol. 43*, 95–160.
Rigler, R., & Ehrenberg, M. (1973) *Q. Rev. Biophys. 6*, 139–199.
Satyshur, K. A., Rao, S. T., Pyalska, D., Drendel, W., Greaser, M., & Sundaralingam, M. (1988) *J. Biol. Chem. 263*, 1628–1647.
Schiefer, S. (1985) in *Methods of Enzymatic Analysis* (Bergmeyer, H. U., Ed.) 3rd ed., Vol. 9, pp 317–331, VCH, Weinheim, Germany, and Deerfield Beach, Florida.
Seamon, K. B. (1980) *Biochemistry 19*, 207–215.
Seeholzer, S. H., & Wand, A. J. (1989) *Biochemistry 28*, 4011–4020.
Small, E. W., & Anderson, S. R. (1988) *Biochemistry 27*, 419–428.
Steiner, R. F., & Norris, L. (1987) *Biophys. Chem. 27*, 27–38.
Szilagyi, L., & Jardetsky, O. (1989) *J. Magn. Reson. 83*, 441–445.
Thulin, E., Andersson, A., Drakenberg, T., Forsen, S., & Vogel, H. J. (1984) *Biochemistry 23*, 1862–1870.
Trewhella, J., Liddle, W. K., Heidorn, D. B., & Strynadka, N. (1989) *Biochemistry 28*, 1294–1301.
Trewhella, J., Blumenthal, D. K., Rokop, S. E., & Seeger, P. A. (1990) *Biochemistry 29*, 9316–9324.
Wagner, G., & Wüthrich, K. (1979) *J. Magn. Reson. 33*, 675–680.
Wang, C. K., Liao, R., Johnson, I., Hudson, B., & Cheung, H. C. (1988) *Biophys. J. 53*, 73a.
Wang, C.-L. A. (1989) *Biochemistry 28*, 4816–4820.
Wang, C.-L. A., Zhan, Q., Tao, T., & Gergely, J. (1987) *J. Biol. Chem. 262*, 9636–9640.
Yazawa, M., Sakuma, M., & Yagi, K. (1980) *J. Biochem. (Tokyo) 87*, 1313–1320.